Magnetic Moment Orientation-Dependent Spin Dissipation in Antiferromagnets

Takahiro Moriyama,* Michinari Kamiya, Kent Oda, Kensho Tanaka, Kab-Jin Kim, and Teruo Ono†
Institute for Chemical Research, Kyoto University, Gokasho, Uji, Kyoto 611-0011, Japan
(Received 3 August 2017; revised manuscript received 10 October 2017; published 29 December 2017)

Spin interaction in antiferromagnetic materials is of central interest in the recently emerging antiferromagnetic spintronics. In this Letter, we explore the spin current interaction in antiferromagnetic FeMn by the spin pumping effect. Exchange biased FeNi/FeMn films, in which the Néel vector can be presumably controlled via the exchange spring effect, are employed to investigate the damping enhancement depending on the relative orientation between the Néel vector and the polarization of the pumped spin current. The correlation between the enhanced damping and the strength of the exchange bias suggests that the twisting of the Néel vector induces an additional spin dissipation, which verifies that the Slonczewski-type spin torque is effective even in antiferromagnetic materials.

DOI: 10.1103/PhysRevLett.119.267204

Itinerant electron spin interacts with local magnetic moments. Upon interaction, the angular momentum of the electron spin is transferred to the local magnetic moments. Consequently, the electron spin exerts a torque on the local magnetic moments. This phenomenon is well known as the spin-torque effect [1,2] and is of great interest not only from the viewpoint of fundamental physics, but also energy efficient spintronic applications, as the spin-torque effect requires much smaller energy to control the magnetization in nanoscale devices than the traditional Ampère field. A wide variety of ferromagnets (FMs) have been employed so far to study the spin-torque effect, and they have already been implemented in actual spintronic devices, such as magnetic random access memory [3].

On the other hand, most of the antiferromagnets (AFMs) have long been abandoned in the studies of the spin-torque effect because they have no net magnetization and it is especially difficult to conduct experimental investigations. Only recent pioneering works [4–13] have been raising attention to the antiferromagnetic spintronics, which can potentially yield fascinating applications such as ultra-high-density magnetic memories [6] and terahertz emission devices [14]. The clear experimental observation of AFM anisotropic magnetoresistance provides a means for detecting electrically the orientation of AFM magnetization [12,13]. Most interestingly and importantly, the demonstration of electrical control of AFM magnetic moments by the spin-orbit interaction in structural inversion symmetry broken systems is of great impact in antiferromagnetic spintronics [7]. Therefore, electrically detecting and controlling magnetic moments in AFMs, which were previously impossible, are now becoming possible. However, these experiments deal with particular materials, which generally require single crystal growth, in order to observe these results. From the viewpoint of AFM spintronic applications, it is more desirable to demonstrate the same in AFMs typically used in spintronic devices such as IrMn, FeMn, and NiO. The universality of spin-torque control of general AFM materials has not been experimentally proven yet. How the electron spins interact with the microscopic magnetic moments of AFM has yet to be fully elucidated experimentally, despite a number of theoretical predictions [15–18].

In ferromagnetic materials, spin interactions and spin torque have been quantitatively investigated by various measurement techniques, including spin-torque switching experiments [19–21] and ferromagnetic resonance (FMR)-based experiments such as spin-torque FMR and spin pumping [22–26]. These techniques are all based on the equation of motion [27,28] for magnetization, with the spin interactions written as

$$\frac{d\mathbf{m}}{dt} = -\gamma \mathbf{m} \times \mathbf{H_{eff}} + \gamma\alpha \mathbf{m} \times \mathbf{H_{eff}} \times \mathbf{m} + \frac{\gamma}{M_s V} \mathbf{m} \times \mathbf{P}_s \times \mathbf{m}, \quad (1)$$

where $\mathbf{m}$ is a unit vector representing the direction of the magnetization with magnitude M_s, γ is the gyromagnetic ratio, $\mathbf{H_{eff}}$ is the effective field applied to the magnetization, α is the Gilbert damping constant, V is the volume of the ferromagnet, and $\mathbf{P}_s$ is the spin current polarization interacting with the magnetization. The third term, proposed by Slonczewski [1], represents the spin torque given to the magnetization. It is noticeable that the spin-torque term is maximal when $\mathbf{m}$ and $\mathbf{P}_s$ are orthogonal, and it is zero when they are parallel. Naturally, this equation works only for FMs, in which only one magnetic unit vector $\mathbf{m}$ can represent the whole magnetic moment in the system. This cannot simply apply to AFMs, as they have another degree of freedom in addition to the magnetic vector $\mathbf{m}$, which is the Néel vector $\mathbf{l}$. For instance, considering the simplest case of a bipartite AFM with two magnetic sublattices having microscopic magnetic moments $\mathbf{m}_1$

and $\mathbf{m}_2$, where the magnetic vector and the Néel vector are, respectively, defined as $\mathbf{m} = \mathbf{m}_1 + \mathbf{m}_2$ and $\mathbf{l} = \mathbf{m}_1 - \mathbf{m}_2$, two sets of equations can be derived for the dynamics [17]. In the quasi-steady-state case with $\mathbf{m} \ll \mathbf{l}$, the spin torque acting on the magnetic vector $\mathbf{m}$ is

$$\left.\frac{d\mathbf{m}}{dt}\right|_{\text{spin torque}} \propto \mathbf{l} \times \mathbf{P_s} \times \mathbf{l} \tag{2}$$

$$= \mathbf{m}_1 \times \mathbf{P_s} \times \mathbf{m}_1 + \mathbf{m}_2 \times \mathbf{P_s} \times \mathbf{m}_2. \tag{3}$$

Equations (2) and (3) clearly show that the spin torque in AFMs also depends on the relative angle between the microscopic magnetic moments (or the Néel vector) and the spin current polarization. The spin torque is maximal when they are orthogonal, in the same manner as in the FM case. Therefore, it is shown mathematically that spin interaction and spin torque exist in AFMs. From the standpoint of the electron, upon spin-torque transfer, the electrons lose (or dissipate) the spin angular momentum [29]. Equation (3) basically suggests that the dissipation of the spin angular momentum depends on the relative angle between $\mathbf{P_s}$ and the microscopic magnetic moments in AFM.

In this Letter, we make use of the exchange biased FM-AFM layer, in which the direction of the Néel vector can be presumably controlled via the exchange spring effect [30,31]. A ferromagnetic resonance measurement was performed with a particular focus on the change of the magnetic damping constant as a function of the relative angle between the FM magnetization and the exchange bias direction, which the AFM Néel vector follows. The results were discussed analogously to the well-known spin pumping experiments performed on FeNi/Cu/Pt multilayers by Mizukami *et al.* [25]. In the spin pumping theory [32], the magnetic dynamics in the FM layer pumps a pure spin current into an adjacent layer whose polarization $\mathbf{P_s}$ is parallel to the equilibrium direction of the FM magnetization. Depending on the extent of spin dissipation in the adjacent layer material, the Gilbert damping constant of the FM layer is modified. In other words, the modification of the damping constant directly infers the spin interaction of the AFM in our experiment.

We prepared Pt 5/$Fe_{50}Mn_{50}$ t/$Fe_{20}Ni_{80}$ 4 /SiO_x 2 nm ($t = 0 \sim 60$ nm) multilayers on a thermally oxidized Si substrate. The thin films were grown by rf magnetron sputtering with a base pressure of 7×10^{-6} Pa at room temperature. The films were then photolithographically patterned into a 10-μm-wide and 20-μm-long strip attached to a coplanar waveguide made of a Ti/Au layer. A field cooling with a temperature of $T_{\text{FC}} = 200\,^{\circ}\text{C}$ and a field of $H_{\text{FC}} = 2$ kOe was performed to define and enhance the exchange bias. The direction of the exchange bias H_{eb}, if acquired, was confirmed to be always in the direction of H_{FC}. In order to carry out a sensitive FMR measurement, we employed a homodyne detection technique [24,33,34] as shown in Fig. 1(a) with the rf circuitry. The measurements were performed at room temperature by sweeping an external magnetic field applied in the sample plane. Since the external magnetic field is sufficiently large compared with the in-plain anisotropy field of the FeNi (including the exchange bias field of ~250 Oe), in the FMR measurement, the magnetization of the FeNi always points in the direction of the external field. Figure 1(a) also indicates the definition of the coordinate system and the angles β, θ, and φ. β is the relative angle between the positive x axis and the direction of H_{eb}. θ is the angle made by the external field, therefore, the magnetization of the FeNi and the positive x axis. Furthermore, $\varphi = \beta - \theta$ is defined as the relative angle between the FeNi magnetization and the direction of H_{eb}. Figure 1(b) shows a typical FMR spectra at 13 GHz in Pt 5 /FeMn 10 /FeNi 4 /SiO_x 2 nm with $\varphi = 15°$ and 195°. The spectrum is well fitted by the combination of symmetric and antisymmetric Lorentzians, from which the resonant parameters, such as the resonant frequency H_{res} and the spectral linewidth ΔH, can be obtained [24]. As shown in the direct comparison in Fig. 1(b), the spectral linewidths ΔH for $\varphi = 15°$ and 195° are visually different, as they are obtained differently from the Lorentzian fitting. H_{res} is plotted against the frequency f in Fig. 1(c). Because there is a unidirectional magnetic anisotropy due to the exchange bias, and the magnetocrystalline anisotropy is negligible in our system, the H_{res} vs f curves vary with φ. We used the following Kittel equation to determine the exchange bias field H_{eb} and the effective demagnetizing field $4\pi M_{\text{eff}}$,

$$f = \frac{\gamma}{2\pi}\sqrt{(H_{\text{res}} + H_{\text{eb}}\cos\varphi)(H_{\text{res}} + 4\pi M_{\text{eff}})}. \tag{4}$$

The Gilbert damping constant α is obtained from the ΔH vs f plot by [35]

$$\Delta H = \Delta H_0 + \frac{2\pi\alpha f}{\gamma}, \tag{5}$$

where ΔH_0 is a frequency-independent linewidth known as the inhomogeneous broadening, which originates from magnetic nonuniformity [36]. Note that the analysis with Eq. (5) explicitly separates the frequency-dependent damping α from the independent one, which may be related to the two-magnon scattering enhanced by inhomogeneities at the FM-AFM interface [37,38]. The variation of the slope of the linear fitting in Fig. 1(d) indicates a significant dependence of α on φ. The spin pumping analyses thereafter were performed based on α as the spin current pumped by the uniformly precessing magnetization which primarily influences α [32]. We note that α obtained here is not influenced by the spin Hall effect of either the FeMn or the Pt since we do not flow dc current in the FMR measurement [39].

In the following, we will discuss the results, particularly with respect to φ, as it was confirmed by a series of separate

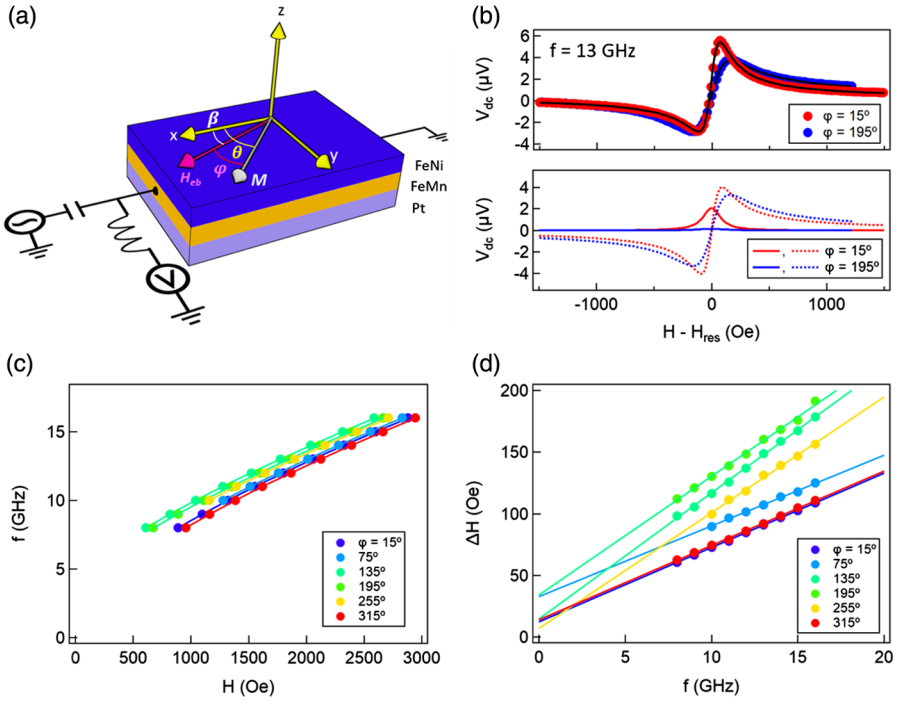

FIG. 1. (a) Schematic illustration of the homodyne detection FMR setup and the definition of the coordinate system. (b) FMR spectra at 13 GHz with $\varphi = 15°$ and 195° fitted by the Lorentzian functions (upper) and the components of symmetric and antisymmetric Lorentzians used in the fitting (lower). (c) Resonant frequency as a function of applied field (markers). The curves are the fitting by Eq. (4). (d) Spectral linewidth ΔH as a function of frequency for Pt 5 /FeMn 10 /FeNi 4 /SiO_x 2 nm fitted by Eq. (5).

experiments (see Supplemental Material [49]), that the damping constant correlates only with φ and has no direct correlation with other angles β or θ. We also ruled out a possibility of damping constant deterioration due to iterations of the field cooling process (see also Supplemental Material [40]).

Figure 2(a) shows α as a function of φ for various thicknesses $t_{\mathrm{FeMn}} = 0$, 10, 20, and 60 nm in Pt 5 /FeMn t_{FeMn}/FeNi 4 /SiO_x 2 nm; α shows a remarkable increase in $\varphi \sim 90$–$270°$ for $t_{\mathrm{FeMn}} = 10$ and 20 nm and shows only a little deviation for $t_{\mathrm{FeMn}} = 60$ nm. As one expects, there is no appreciable variation of α with φ in the control sample with $t_{\mathrm{FeMn}} = 0$ nm. The increase of α seems to be related to the strength of H_{eb} as one can see the t_{FeMn} dependence of H_{eb}, shown in Fig. 2(b), obtained by FMR analysis based on Eq. (4). H_{eb} emerges above $t_{\mathrm{FeMn}} = 5$ nm and shows the maximum value of $H_{\mathrm{eb}} = 230$ Oe at around $t_{\mathrm{FeMn}} = 10$ nm. Above $t_{\mathrm{FeMn}} = 10$ nm, it shows a monotonic decrease. The inset of Fig. 2(b) shows $4\pi M_{\mathrm{eff}}$, obtained from FMR data by fitting with Eq. (4), as a function of FeMn thickness. The $4\pi M_{\mathrm{eff}}$ is essentially independent of the FeMn thickness and it is 0.89 ± 0.06 T, which is reasonably accounted for as the demagnetizing field of the FeNi, for which the saturation magnetization was separately measured to be $(7.0 \pm 0.2) \times 10^6$ A/m. This implies that, regardless of the strength of H_{eb} or the thickness of the FeMn, the magnetization dynamics detected in this experiment is mainly from the FeNi.

The mechanism of exchange bias is generally explained by two major factors [31]. One is the exchange coupling at the FM-AFM interface, the strength of which depends sensitively on the quality of the interface morphology. The other is the magnetic anisotropy energy of the AFM, which decays as the AFM thickness decreases. Therefore, we consider three regimes for the appearance of exchange bias in our systems: (I) With $t_{\mathrm{FeMn}} < 5$ nm, FeNi and FeMn are strongly exchange coupled but the anisotropy energy of the FeMn is so small that the magnetic moments of FeNi and FeMn rotate together. Consequently, no exchange bias is observed. (II) With $t_{\mathrm{FeMn}} \sim 10$ nm, FeNi and FeMn are strongly exchange coupled and the anisotropy of the FeMn is sufficiently large to induce the exchange bias. Rotation of

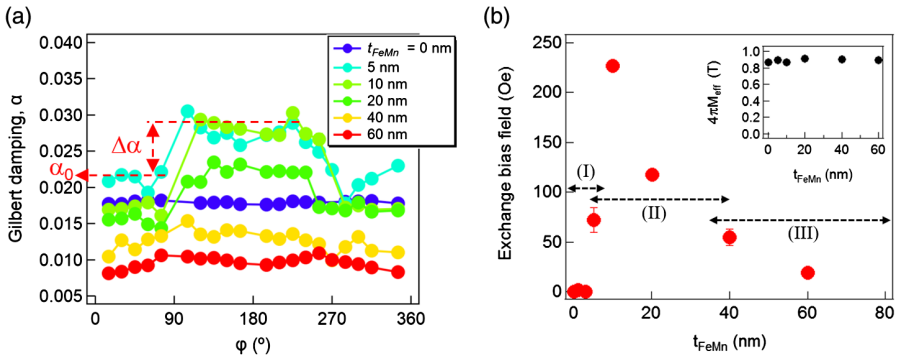

FIG. 2. (a) Gilbert damping α as a function of the relative angle φ for Pt 5 /FeMn t_{FeMn}/FeNi 4 /SiO_x 2 nm with $t_{\mathrm{FeMn}} = 0$, 5, 10, 20, 40, and 60 nm. The definitions of α_0 and $\Delta\alpha$ are indicated. (b) Exchange bias field H_{eb} as a function of t_{FeMn}. Regimes I, II, and III described in the main text are indicated by the double sided arrows. The inset shows the t_{FeMn} dependence of $4\pi M_{\mathrm{eff}}$.

the FeNi magnetization gives rise to a twist of the Néel vector in the FeMn [30]. (III) With $t_{\mathrm{FeMn}} > 20$ nm, the exchange coupling at the FeNi/FeMn interface deteriorates due to a change in the interfacial morphology [41], and the FeNi and FeMn are magnetically decoupled.

We now define the baseline of α as α_0 and the increase of α as $\Delta\alpha$, as depicted in Fig. 2(a). α_0 represents the magnetic damping when the equilibrium magnetization direction of FeNi is in the same direction as the exchange bias field. $\Delta\alpha$ represents the maximum change of the magnetic damping when the equilibrium magnetization direction of FeNi is away from the direction of H_{eb}. As shown in Fig. 3(a), α_0 decreases with increasing the FeMn thickness with a similar trend seen in a previous work on FeNi/Cu/Pt systems [25]. In the framework of the spin pumping theory, the layer structure of our system can be modeled as follows: the FeNi magnetization dynamics pumps the spin current and injects it into the FeMn layer, the spin current then diffuses in the FeMn layer, and the 5 nm Pt layer works as a good spin sink. Assuming that the spin current in the FeMn is dissipated over a certain length (spin diffusion length) λ_{FeMn}, the enhancement of the magnetic damping $\delta\alpha$ due to the spin pumping effect can be written as [32]

$$\delta\alpha = \alpha_0 - \alpha_{\mathrm{int}} = \left(1 + \tilde{g}_r^{\uparrow\downarrow} R_{\mathrm{sd}} \frac{1 + \tanh(t_{\mathrm{FeMn}}/\lambda_{\mathrm{FeMn}})\tilde{g}R_{\mathrm{sd}}}{\tanh(t_{\mathrm{FeMn}}/\lambda_{\mathrm{FeMn}})\tilde{g}R_{\mathrm{sd}}}\right)^{-1} \frac{\hbar\gamma^2\tilde{g}_r^{\uparrow\downarrow}}{4\pi t_{\mathrm{FeNi}}}, \tag{6}$$

where $\hbar$ is the reduced Planck constant, t_{FeNi} is the thickness of the FeNi layer, and α_{int} is the intrinsic damping of the FeNi, which was measured separately to be $\alpha_{\mathrm{int}} = 0.008$; $\tilde{g}_r^{\uparrow\downarrow}$ and $\tilde{g}$ are the mixing conductance per unit area of the FeNi/FeMn interface and the FeMn/Pt interface, respectively. $R_{\mathrm{sd}}^{-1} \approx 2\tilde{g}_r^{\uparrow\downarrow}\sqrt{\epsilon/3}$, where ϵ is the ratio of the momentum to the spin-flip scattering time. The dotted lines overlaid in Fig. 3(a) are the values of α_0 calculated by Eq. (6) with $\lambda_{\mathrm{FeMn}} = 50$, 100, and 200 nm; $\tilde{g}_r^{\uparrow\downarrow} \sim 0.3 \times 10^{18}$ m^{-2}, $\tilde{g} \sim 0.5 \times 10^{18}$ m^{-2}, and $\epsilon \sim 10^{-2}$, which are within reasonable values compared with the previously reported ones for metallic systems [42,43], are chosen so that they reproduce the experimentally measured α_0 trend. It is noticeable that a little deviation of parameters $\tilde{g}_r^{\uparrow\downarrow}$, $\tilde{g}$, and ϵ does not influence the asymptotic behavior of α_0 with respect to t_{FeMn}, as it is predominantly determined by λ_{FeMn}. We therefore point out that the obtained FeMn thickness dependence of α_0 suggests that λ_{FeMn} can be more than an order of magnitude larger than the values reported in Refs. [44–46], but are more consistent with Refs. [11,47], indicating that λ_{FeMn} may be enhanced by the magnon carrying the spin current [9–11,48]. Indeed, the previous experiments reporting the shorter spin diffusion lengths seem to have been performed with disordered Néel vectors. In our present measurements, on the contrary, α_0 is measured when the Néel vector of the FeMn is presumably aligned with $\mathbf{P}_{\mathbf{s}}$ pumped from the FeNi. Therefore, the alignment of the Néel vector and $\mathbf{P}_{\mathbf{s}}$ can be a key for obtaining a longer spin diffusion length in AFMs.

Compared with the variation of α_0, $\Delta\alpha$ shows a quite different trend, as shown in the inset of Fig. 3(b). It approaches zero in both the thick and the thin limits and peaks at around $t_{\mathrm{FeMn}} = 10$ nm, which cannot be attributed to the simple exponentially decaying spin diffusion process described by Eq. (6). Figure 3(b) shows that $\Delta\alpha$ and the exchange bias field H_{eb} indeed render a nice linear correlation. This correlation can be explained by a damping enhancement due to an additional spin dissipation depending on the relative angle between the Néel vector and $\mathbf{P}_{\mathbf{s}}$, as indicated in Eq. (2). Namely, in regime I, the alignment of the Néel vector and $\mathbf{P}_{\mathbf{s}}$ is maintained regardless of $s\varphi$. Therefore, no additional damping is observed. In regime II, the Néel vector twisting upon the rotation of FeNi magnetization increases the spin dissipation. Therefore, an additional damping depending on φ is observed. In regime III, since the exchange coupling is weak, only small exchange bias is induced. The majority of the antiferromagnetic domains are still randomly oriented even after the field cooling, as described in the Supplemental Material [40]. Therefore, the Néel vector orientations on average remain invariant under the rotation of FeNi magnetization. In such a case, there should not be any damping change observed with respect to φ. With the above arguments, we believe that the twisting of the FeMn Néel vector is the

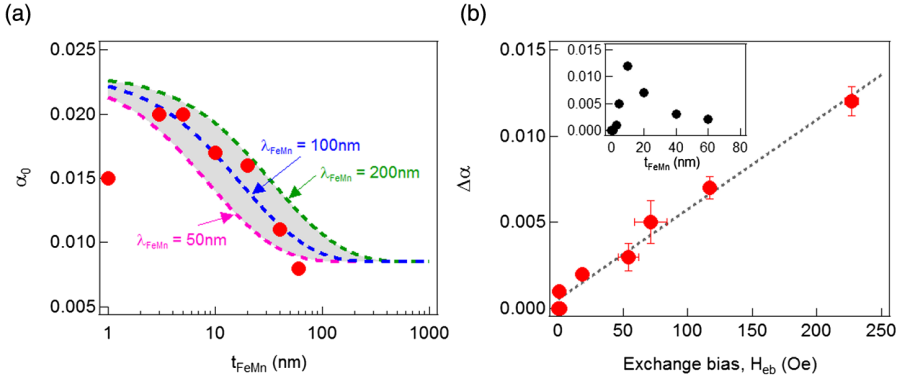

FIG. 3. (a) α_0 as a function of t_{FeMn}. Dotted lines, superimposed on the experimental data points, are calculated by Eq. (6) with $\lambda_{\mathrm{FeMn}} = 50$, 100, and 200 nm. (b) $\Delta\alpha$ as a function of the exchange bias field H_{eb}. The inset shows $\Delta\alpha$ as a function of the FeMn thickness.

source of the additional spin dissipation, which is interpreted such that, even in AFM, the spin current dissipation clearly depends on the relative angle between the microscopic magnetic moments (or the Néel vector) and $\mathbf{P}_s$. These results suggest that Eq. (3) is generally true and the Slonczewski-type spin torque is effective in AFM. Finally, it should be noted that, if the Néel vector smoothly rotated with φ, the damping would smoothly vary with φ, contrary to what is shown in Fig. 2(a). This rather abrupt enhancement of α in $\varphi = \sim 90$–$270°$ implies that the twisting of the Néel vector may be relaxed by accommodating the domain walls in AFM, as suggested in Refs. [31,49].

In summary, we investigated the magnetic damping enhancement in Pt/FeMn/FeNi/SiO_x with respect to the relative angle between the FeNi magnetization and the direction of the exchange bias. The results were discussed based on the spin pumping theory. The correlation between the enhanced damping and the strength of the exchange bias strongly suggests that the twisting of the Néel vector induces the damping enhancement, which verifies that the Slonczewski-type spin torque is effective even in antiferromagnetic materials. Our experimental results enable the use of the spin-torque effect in more general antiferromagnetic materials in the framework of the antiferromagnetic spintronics.

This work was supported in part by JSPS KAKENHI Grants No. 26870300, No. 17H04924, No. 15H05702, and No. 17H05181 ("Nano Spin Conversion Science"). We also acknowledge the support from the Center for Spintronics Research Network (CSRN).

*mtaka@scl.kyoto-u.ac.jp
†ono@scl.kyoto-u.ac.jp

[1] J. C. Slonczewski, J. Magn. Magn. Mater. **159**, L1 (1996).
[2] L. Berger, Phys. Rev. B **54**, 9353 (1996).
[3] J. A. Katine and E. E. Fullerton, J. Magn. Magn. Mater. **320**, 1217 (2008).
[4] Z. Wei, A. Sharma, A. S. Nunez, P. M. Haney, R. A. Duine, J. Bass, A. H. MacDonald, and M. Tsoi, Phys. Rev. Lett. **98**, 116603 (2007).
[5] S. Urazhdin and N. Anthony, Phys. Rev. Lett. **99**, 046602 (2007).
[6] S. Loth, S. Baumann, C. P. Lutz, D. M. Eigler, and A. J. Heinrich, Science **335**, 196 (2012).
[7] P. Wadley *et al.*, Science **351**, 587 (2016).
[8] S. Nakatsuji, N. Kiyohara, and T. Higo, Nature (London) **527**, 212 (2015).
[9] H. Wang, C. Du, P. C. Hammel, and F. Yang, Phys. Rev. Lett. **113**, 097202 (2014).
[10] C. Hahn, G. de Loubens, V. V. Naletov, J. B. Youssef, O. Klein, and M. Viret, Europhys. Lett. **108**, 57005 (2014).
[11] T. Moriyama, S. Takei, M. Nagata, Y. Yoshimura, N. Matsuzaki, T. Terashima, Y. Tserkovnyak, and T. Ono, Appl. Phys. Lett. **106**, 162406 (2015).
[12] X. Marti *et al.*, Nat. Mater. **13**, 367 (2014).
[13] T. Moriyama, N. Matsuzaki, K.-J. Kim, I. Suzuki, T. Taniyama, and T. Ono, Appl. Phys. Lett. **107**, 122403 (2015).
[14] R. Cheng, D. Xiao, and A. Brataas, Phys. Rev. Lett. **116**, 207603 (2016).
[15] A. S. Nunez, R. A. Duine, P. Haney, and A. H. MacDonald, Phys. Rev. B **73**, 214426 (2006).
[16] P. M. Haney and A. H. MacDonald, Phys. Rev. Lett. **100**, 196801 (2008).
[17] H. V. Gomonay and V. M. Loktev, Phys. Rev. B **81**, 144427 (2010).
[18] R. Cheng and Q. Niu, Phys. Rev. B **86**, 245118 (2012).
[19] J. Z. Sun, Phys. Rev. B **62**, 570 (2000).
[20] F. J. Albert, N. C. Emley, E. B. Myers, D. C. Ralph, and R. A. Buhrman, Phys. Rev. Lett. **89**, 226802 (2002).
[21] J. A. Katine, F. J. Albert, R. A. Buhrman, E. B. Myers, and D. C. Ralph, Phys. Rev. Lett. **84**, 3149 (2000).
[22] J. C. Sankey, P. M. Braganca, A. G. F. Garcia, I. N. Krivorotov, R. A. Buhrman, and D. C. Ralph, Phys. Rev. Lett. **96**, 227601 (2006).
[23] H. Kubota, A. Fukushima, K. Yakushiji, T. Nagahama, S. Yuasa, K. Ando, H. Maehara, Y. Nagamine, K. Tsunekawa, D. D. Djayaprawira, N. Watanabe, and Y. Suzuki, Nat. Phys. **4**, 37 (2008).
[24] L. Liu, T. Moriyama, D. C. Ralph, and R. A. Buhrman, Phys. Rev. Lett. **106**, 036601 (2011).
[25] S. Mizukami, Y. Ando, and T. Miyazaki, Phys. Rev. B **66**, 104413 (2002).
[26] B. Heinrich, Y. Tserkovnyak, G. Woltersdorf, A. Brataas, R. Urban, and G. E. W. Bauer, Phys. Rev. Lett. **90**, 187601 (2003).
[27] L. D. Landau and E. M. Lifshitz, Phys. Z. Sowjetunion **8**, 153 (1935).
[28] T. L. Gilbert, Phys. Rev. **100**, 1243 (1955).
[29] M. D. Stiles and A. Zangwill, Phys. Rev. B **66**, 014407 (2002).
[30] A. Scholl, M. Liberati, E. Arenholz, H. Ohldag, and J. Stöhr, Phys. Rev. Lett. **92**, 247201 (2004).
[31] D. Mauri, H. C. Siegmann, P. S. Bagus, and E. Kay, J. Appl. Phys. **62**, 3047 (1987).
[32] Y. Tserkovnyak, A. Brataas, G. E. W. Bauer, and B. I. Halperin, Rev. Mod. Phys. **77**, 1375 (2005).
[33] K. Tanaka, T. Moriyama, M. Nagata, T. Seki, K. Takanashi, S. Takahashi, and T. Ono, Appl. Phys. Express **7**, 063010 (2014).
[34] H. Mizuno, T. Moriyama, M. Kawaguchi, M. Nagata, K. Tanaka, T. Koyama, D. Chiba, and T. Ono, Appl. Phys. Express **8**, 073003 (2015).
[35] B. Heinrich, J. F. Cochran, and R. Hasegawa, J. Appl. Phys. **57**, 3690 (1985).
[36] R. Arias and D. L. Mills, Phys. Rev. B **60**, 7395 (1999).
[37] S. M. Rezende, A. Azevedo, M. A. Lucena, and F. M. de Aguiar, Phys. Rev. B **63**, 214418 (2001).
[38] M. C. Weber, H. Nembach, B. Hillebrands, and J. Fassbender, J. Appl. Phys. **97**, 10A701 (2005).
[39] We only flow an rf charge current in the device in our homodyne FMR measurements. The rf charge current would give rise to the "rf" spin current due to the spin Hall effect (SHE) in the FeMn or Pt. However, since the time

average of the rf spin current is zero, it cannot reduce or enhance the total spin angular momentum of the system. Therefore, the Gilbert damping, which reflects the spin angular momentum of the system, should not be affected by the SHE.

[40] See Supplemental Material at http://link.aps.org/supplemental/10.1103/PhysRevLett.119.267204 for supporting data.

[41] J. Wang, T. Sannomiya, J. Shi, and Y. Nakamura, J. Appl. Phys. **113**, 17D707 (2013).

[42] Y. Yang, Y. Xu, K. Yao, and Y. Wu, AIP Adv. **6**, 065203 (2016).

[43] M. Tokaç, S. A. Bunyaev, G. N. Kakazei, D. S. Schmool, D. Atkinson, and A. T. Hindmarch, Phys. Rev. Lett. **115**, 056601 (2015).

[44] W. Zhang, M. B. Jungfleisch, W. Jiang, J. E. Pearson, A. Hoffmann, F. Freimuth, and Y. Mokrousov, Phys. Rev. Lett. **113**, 196602 (2014).

[45] P. Merodio, A. Ghosh, C. Lemonias, E. Gautier, U. Ebels, M. Chshiev, H. Béa, V. Baltz, and W. E. Bailey, Appl. Phys. Lett. **104**, 032406 (2014).

[46] Y. Yang, Y. Xu, X. Zhang, Y. Wang, S. Zhang, R.-W. Li, M. S. Mirshekarloo, K. Yao, and Y. Wu, Phys. Rev. B **93**, 094402 (2016).

[47] T. Moriyama, M. Nagata, K. Tanaka, K-J. Kim, H. Almasi, W. Wang, and T. Ono, arXiv:1411.4100.

[48] S. Takei, T. Moriyama, T. Ono, and Y. Tserkovnyak, Phys. Rev. B **92**, 020409(R) (2015).

[49] J. Li, A. Tan, S. Ma, R. F. Yang, E. Arenholz, C. Hwang, and Z. Q. Qiu, Phys. Rev. Lett. **113**, 147207 (2014).